

UC San Diego

UC San Diego Previously Published Works

Title

Development of a Potent Inhibitor of the Plasmodium Proteasome with Reduced Mammalian Toxicity

Permalink

<https://escholarship.org/uc/item/0r57k1b0>

Journal

Journal of Medicinal Chemistry, 60(15)

ISSN

0022-2623

Authors

LaMonte, Gregory M
Almaliti, Jehad
Bibo-Verdugo, Betsaida
[et al.](#)

Publication Date

2017-08-10

DOI

10.1021/acs.jmedchem.7b00671

Copyright Information

This work is made available under the terms of a Creative Commons Attribution-NonCommercial-NoDerivatives License, available at <https://creativecommons.org/licenses/by-nc-nd/4.0/>

Peer reviewed

Development of a potent inhibitor of the *Plasmodium* proteasome with reduced mammalian toxicity

Gregory M. LaMonte^{1§}, Jehad Almaliti^{3§}, Betsaida Bibo-Verdugo^{2§}, Lena Keller^{3§}, Bing Yu Zou¹, Jennifer Yang¹, Yevgeniya Antonova-Koch¹, Pamela Orjuela-Sanchez¹, Colleen A. Boyle¹, Edgar Vigil¹, Lawrence Wang¹, Gregory M. Goldgof¹, Lena Gerwick², Anthony J. O'Donoghue^{2*}, Elizabeth A. Winzeler^{1*}, William H. Gerwick^{2,3*} and Sabine Otilie^{1*}

¹ Department of Pediatrics, University of California, San Diego, School of Medicine, La Jolla, CA 92093, United States

² Skaggs School of Pharmacy and Pharmaceutical Sciences, Faculty of Pharmacy, University of California, San Diego, School of Medicine, La Jolla, CA 92093, USA

³ Scripps Institution of Oceanography, University of California, San Diego, La Jolla, CA 92093, USA.

§ These authors contributed equally to the project

* Corresponding authors (AJO for proteasome, EW for malaria, WHG for chemistry, SO for resistance and toxicity)

Keywords: Malaria, Proteasome Inhibitors, Natural Products

Abstract

Naturally derived chemical compounds are the foundation of much of our pharmacopeia, especially in anti-proliferative and anti-infective drug classes. Natural products have been a valuable source of chemically diverse antimalarial compounds too. Here, we report that a naturally-derived molecule called carmaphycin B, is a potent inhibitor against both the asexual and sexual blood stages of malaria infection. Using a combination of *in silico* molecular docking and *in vitro* directed evolution in a well-characterized drug-sensitive yeast model, we determined that these compounds target the $\beta 5$ subunit of the proteasome. These studies were validated using *in vitro* inhibition assays with proteasomes isolated from *Plasmodium falciparum*. As carmaphycin B is toxic to mammalian cells, we synthesized a series of chemical analogs that reduce host cell toxicity while maintaining blood-stage and gametocytocidal antimalarial activity and proteasome inhibition. This study describes a promising new class of antimalarial compound based on the carmaphycin B scaffold, as well as several chemical structural features that serve to enhance antimalarial specificity.

Introduction

Despite extensive public health interventions ¹, malaria continues to be a major global health challenge, resulting in millions of infections per year and 438,000 deaths, predominantly children under the age of 5 years. Furthermore, as the efficacy of artemisinin combination therapies continue to wane due to the emergence of drug resistant strains ²⁻³, it is feared that malaria will continue to expand and cause significant hardships worldwide. This onset of drug resistance highlights the urgent need for developing new and potent antimalarial compounds with novel mechanisms of action. In particular, there has been a significant focus on identifying compounds which possess transmission blocking or prophylactic activity, rather than the traditional focus on blood-stage infection. In the last 5-10 years, numerous phenotypic screens have been undertaken which have identified several novel antimalarial compounds ⁴. More recently, as part of the effort to increase the utility of those screens, there has been a search for increased chemical diversity in a variety of parasitic species, such as through the introduction of the Global Health Chemical Diversity and Diversity-oriented Synthesis libraries ⁵⁻⁶, to increase the chance of identifying novel antimalarial chemotypes which can affect multiple stages of parasite development.

One often utilized source of chemical diversity are natural products, which have been successful in screening programs as they often possess distinct chemical structures that have proven to be a valuable resource for anti-cancer, anti-hypertension and anti-microbial compounds ⁷. Several of the most prominent antimalarial compounds, including quinine and artemisinin were isolated from natural sources ⁸. Here, we report a new series of compounds, with potent antimalarial activity against the sexual and asexual lifecycle stages, derived from the natural product carmaphycin B.

Carmaphycin B and a related compound carmaphycin A, were originally isolated from extracts derived from cyanobacterium *Symploca* sp. obtained from Curaçao ⁹. They are tripeptide molecules, capped on the amino terminus with an N-hexanoyl group and an α,β -epoxyketone group on the carboxyl terminus. Carmaphycin B consists of L-valine, L-methionine sulfone and L-leucine while carmaphycin A has L-methionine sulfoxide instead of the methionine sulfone. Previous work by our group has shown that both compounds elicit a strong cytotoxic effect on a human lung adenocarcinoma and a colon cancer cell line ⁹. This cytotoxic effect is likely due to targeting of the constitutive proteasome, as has been demonstrated with the α,β -epoxyketone inhibitor, carfilzomib. Carfilzomib is an approved drug for treatment of refractory or relapsed multiple myeloma. Carfilzomib also kills asexual blood stage *P. falciparum* ¹⁰ and can strongly synergize artemisinin activity ¹¹. In addition, analogs of carfilzomib have been shown to have oral bioavailability ¹², a critical feature for antimalarial compounds. However, the concentration of carfilzomib required for effective treatment of malaria would be toxic to host cells, and this lack of specificity has largely rendered it unusable from an anti-microbial perspective. A review of the proteasome inhibitors tested against Plasmodium and other protozoan parasites has been described elsewhere ¹³.

A peptide epoxyketone inhibitor with reduced toxicity to *Plasmodium* and host cells was identified in a screen of carfilzomib analogs. This compound had sufficient selectivity to reduce parasite load in *P. berghei* infected mice without host toxicity but was unable to clear parasitemia ¹⁰. These studies confirmed that antimalarial proteasome inhibitors with low host cytotoxicity can be designed, however a significant improvement in anti-malarial potency is needed.

This study reports on our efforts to design and evaluate proteasome inhibitors based on the carmaphycin B scaffold, and to identify analogs that have potent antimalarial activity with low host cytotoxicity. Our lead compound, designated analog **18**, has a 100-fold wider therapeutic window than carmaphycin B and

consists of the substitutions of D-valine for L-valine, and norleucine for methionine sulfone. We show that this compound retains potent antimalarial efficacy in cell based assays against both asexual blood stages and gametocytes, and strongly inhibits the activity of the isolated *Plasmodium* proteasome *in vitro*. *In vitro* evolution in *S. cerevisiae*, biochemical assays and molecular modeling studies confirm that this activity is due to specific inhibition of the $\beta 5$ subunit of the proteasome. We then utilized molecular modeling of these inhibitors with the $\beta 5$ -subunit of the human versus parasite proteasome to demonstrate that subtle structural differences in the $\beta 5$ -subunit active site permit this selectivity. Together, these studies conclusively demonstrate that toxicity of these molecules to human cells can be dramatically reduced while still maintaining potent anti-microbial activity.

Results and Discussion

Target confirmation through *in vitro* directed evolution in yeast

In our previous work, we showed biochemical evidence that carmaphycin B inhibits the $\beta 5$ subunit of the 20S yeast proteasome ⁹. In order to confirm that the cellular mechanism of action of carmaphycin B is through direct binding to the $\beta 5$ subunit and determine residues important for interaction, we used directed evolution of compound resistance in yeast followed by whole genome sequencing. This approach has been used successfully by our group to uncover the molecular targets of antiparasitic compounds and helped to determine amino acids crucial for a given target-compound pair ¹³⁻¹⁴. Directed evolution was performed by exposing a drug-sensitive *S. cerevisiae* strain, lacking 16 multidrug ABC-transporter export pumps (ABC₁₆-Monster strain; GM) ¹⁵, to concentrations of carmaphycin B exceeding the IC₅₀ determined for the parental strain. Three carmaphycin B-resistant clones, termed lineage 1, 2 and 3 were isolated, with >6-, 2.2-, and >4-fold resistance when compared to the parental strain (Table S1). The genetic basis of this resistance was investigated by whole-genome sequencing of the resistant lineages with more than 40-fold coverage (Table S2). The resulting sequences were compared to those of the parental-strain (S288c) reference genome and variants present only in the evolved lines were identified (Table S3).

In each of the three lineages we detected 9, 4 and 15 single nucleotide variants. In the second resistant clone (lineage 2), we identified a nonsynonymous single-nucleotide change in the PRE2 gene that resulted in a

M120I change in the $\beta 5$ subunit of the 20S proteasome, the putative target of carmaphycin B. The $\beta 5$ subunit is synthesized as a pro-protein and residue M120I corresponds to M45I in the mature protein. This same mutation has been identified in the $\beta 5$ subunit of human cell lines after long-term exposure to high doses bortezomib, a proteasome inhibitor used for treatment of multiple myeloma ¹⁶. The two other resistant clones have mutations in genes whose products are involved in the ubiquitin pathway (lineage 1: SNT2 and lineage 3: UBP7 and UBP3) ¹⁷ and might represent compensatory mutations leading to resistance to carmaphycin B. Ubiquitination is known to be a reversible posttranslational modification whereby specialized ubiquitin proteases remove ubiquitin from cellular substrates. Both, UBP7 and UBP3 are encoding deubiquitinating enzymes (DUB) and furthermore, UBP3 has been shown to play a role in 20S proteasome degradation ¹⁸⁻²⁰. Therefore, we speculate that mutations in these two CarB resistant strains confer compensatory resistance by diminishing the deleterious effect of accumulation of ubiquitinated proteins in the presence of carmaphycin B and potentially stabilizing the core 20S proteasome. None of the three lineages contained insertions or deletions relative to the parental strain. Therefore, the available evidence obtained through genetic means further supports that carmaphycin B targets the $\beta 5$ subunit of the proteasome and that a single amino acid substitution abolishes this interaction.

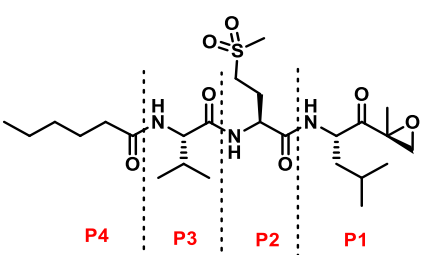
Molecular Docking elucidates target-compound interaction

To better understand how the M45I mutation confers carmaphycin B resistance, the crystal structure of the yeast 20S proteasome in complex with carmaphycin A (PDB ID 4HRD) was used for protein engineering in Molecular Operating Environment (MOE) to obtain the model 4HRD-M45I for the mutated $\beta 5$ subunit (PDB ID 4HRD chain K) ²¹. Comparison of the mutant and wild-type protein structures shows that the mutation does not trigger apparent changes in the overall protein folding, but rather, influences the direct contact between the ligand and the protein. Detailed analysis of the 4HRD-M45I model suggests that a mutation of Met45 to Ile45 leads to a constriction of the S1 pocket and therefore sterically hinders binding of the inhibitor (Figure 1), and therefore explains how this mutation confers resistance to carmaphycin B and confirms the importance of the M45 residue for target-compound interaction ²¹⁻²².

Carmaphycin B exhibits potent sexual and asexual antimalarial activity

Previous studies on epoxyketone containing compounds such as epoxomicin and carfilzomib, have shown that they possess potent antiprotozoal²³ and antimalarial activity against asexual^{10,24}, and sexual blood stages²⁵. Based on its structural similarity, we evaluated the activity of carmaphycin B against the asexual blood stage of *P. falciparum*. We found that the natural product possesses potent asexual blood stage activity, with an IC₅₀ of 4.1 nM ± 0.17 as measured by 72 hour SYBR green assay (Table 2), but also exhibits potent activity against the liver-stage (61.6 nM ± 11) and Stage V gametocytes (160 nM ± 24).

Table 2: Structure and Antimalarial Activity of Carmaphycin B. Results presented as mean ± s.e.m with n=3.

Compound Name	Compound Structure	<i>P. falciparum</i> Dd2 IC ₅₀ (nM)	<i>P. berghei</i> IC ₅₀ (nM)	<i>P. f.</i> Stage V Gametocyte IC ₅₀ (nM)
Carmaphycin B		4.1 ± 0.17	61.6 ± 11	160 ± 24

Several proteasome inhibitors have been reported with antimalarial activity but because the 20S proteasome is a highly conserved target, many are also cytotoxic to human cells²⁶. Similarly, carmaphycin B also exhibits significant cytotoxicity against HepG2 cells (IC₅₀ of 12.6 nM). Li and colleagues attempted to resolve this problem by using substrate specificity information to design a proteasome inhibitor that is 247-fold more selective against *P. falciparum* trophozoites when compared to human fibroblasts. This selective inhibitor, comprised of a tripeptide with a C-terminal vinyl-sulfone reactive group (WLL-vs), irreversibly targets the active site threonine residue of the β5 subunit²⁷. Unfortunately, peptide vinyl sulfone inhibitors are additionally known to target several human cysteine proteases that are ubiquitously expressed in human cells²⁸, leading to potential concerns about off-target specificity. Therefore, we focused our efforts on the exquisite specificity of the epoxyketone reactive group for threonine residues to develop proteasome inhibitors with improved selectivity for the *P. falciparum* 20S proteasome²⁹⁻³⁰.

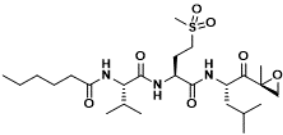
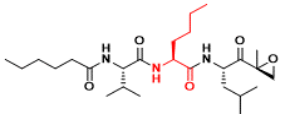
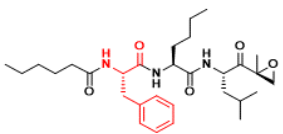
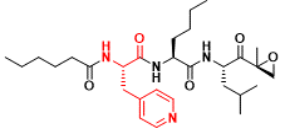
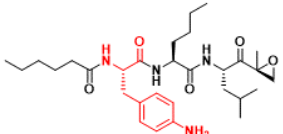
Carmaphycin B (Table 2) is divided into 4 structural subunits; the leucine epoxyketone (EK) (P1), the methionine sulfone (P2), valine (P3) and hexanoic acid (P4) moieties. Our goal was to design chemical analogs consisting of modifications at P1, P2 and P3 that retain potent antimalarial activity but increased specificity. We therefore utilized a convergent, flexible and scalable synthetic procedure that avoids racemization, a common problem in the synthesis of peptide-like structures. Once synthesized, all 20 analogs generated were confirmed to have >95% purity by HPLC.

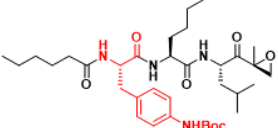
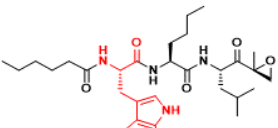
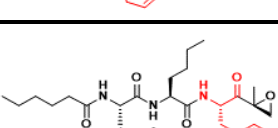
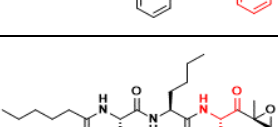
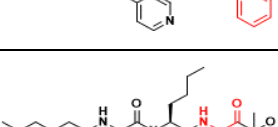
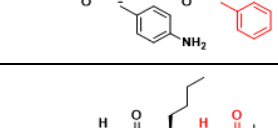
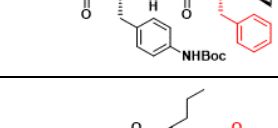
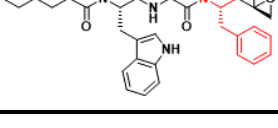
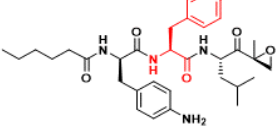
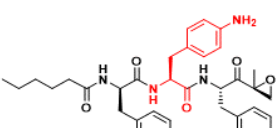
Carmaphycin B and 20 synthetic analogs were assayed for their biological activity against *P. falciparum* and HepG2 cells with the goal of identifying modifications that lead to an increase in the selectivity index relative to carmaphycin B (Table 3). For analog **1**, we changed the methionine sulfone in the P2 position to norleucine residue, in order to explore the importance of a hydrogen bond at this position. Norleucine was chosen because of its similarity in length and flexibility to methionine sulfone. This replacement decreased the cytotoxic activity of carmaphycin B and resulted in a 10-fold increase in selectivity. With compound **1** as a starting point, we designed two groups of carmaphycin analogs.

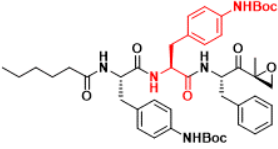
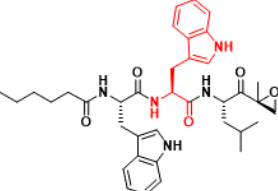
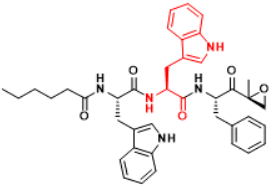
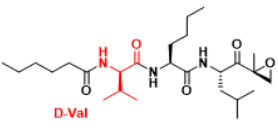
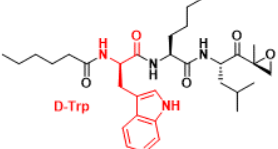
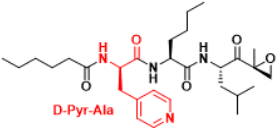
The first group of analogs contained a series of P3 side chains of increasing size: L-phenylalanine (analog **2**), 3-(4-pyridyl)-L-alanine (4-Pyr-L-Ala) (analog **3**), 4-amino-L-phenylalanine (4-NH₂-L-Phe) (analog **4**), 4-(Boc-amino)-L-phenylalanine (analog **5**) (BocNH- L-Phe), and L-tryptophan (L-Trp) (analog **6**). None of these compounds had improved selectivity when compared to analog **1**. The second group of analogs was synthesized using the same selection of P3 amino acids as the first group but substituting L-phenylalanine instead of the original L-leucine residue in the P1 position (analog **7-11**). In a previous study, the *Plasmodium* proteasome showed a clear preference for phenylalanine at the P1 position²⁷. Correspondingly, most compounds with L-Phe at P1 showed an increased selectivity index compared to their L-Leu counterparts. While several of these analogs, particularly analogs **9** and **10**, demonstrated increased selectivity, these analogs showed reduced antimalarial potency relative to analog **1** and therefore were not pursued further. A third group of six analogs, **12-17**, was designed to explore the contribution of bulkier P2 residues in combination with similarly sized P3 residues introduced previously. Unfortunately, none of these 6 analogs demonstrated a better combination of potency and selectivity relative to analog **1**, and were therefore not studied in more detail.

For the last group of analogs (**18-20**), we examined the effect of D-amino acids at the P3 position. In previous studies on specific inhibitors of human immunoproteasomes, it has been shown that D-amino acids can have a strong effect on the overall binding mode of the compound ³¹. We therefore replaced the L-Val of analog **1** with D-Val (analog **18**), D-Trp (analog **19**), and Pyr-D-Ala (analog **20**) in the P3 position. Remarkably, analogs **18** and **19** showed up to 100-fold reduced toxicity together with higher antimalarial potency, resulting in a 100-fold increase in selectivity for analogs **18** and **19**. Overall, our most promising derivative, **18**, shows a 123-fold increase in selectivity index compared to the natural product carmaphycin B while at the same time retaining its potent anti-gametocyte activity, with an IC₅₀ against stage V gametocytes of 130 nM.

Table 3 illustrates carmaphycin B and analogs **1-20** along with their *P. falciparum* asexual blood stage activity and cytotoxicity towards HepG2 cells and the selectivity index (comparing the *P. falciparum* activity versus HepG2 activity). The residue in the chemical structure that changes compared to the previous group of analogs is colored in red. Results presented as mean \pm s.e.m with n=3.

Compound #	Structure	P3	P2	P1	<i>P.falciparum</i> Dd2 IC ₅₀ [nM]	HepG2 IC ₅₀ [nM]	Selectivity Index
Carmaphycin B		L-Val	L-Met-Ox	L-Leu-EK	4.10 \pm 0.17	12.6 \pm 1.40	3.07
1		L-Val	L-Nle	L-Leu-EK	4.11 \pm 0.077	134 \pm 86.7	33.3
2		L-Phe	L-Nle	L-Leu-EK	4.04 \pm 0.76	22.7 \pm 8.42	5.62
3		4-Pyr-L-Ala	L-Nle	L-Leu-EK	3.28 \pm 0.67	< 0.283	0.09
4		4-NH ₂ -L-Phe	L-Nle	L-Leu-EK	5.99 \pm 1.08	6.32 \pm 4.99	1.06

5		4-Boc-NH-L-Phe	L-Nle	L-Leu-EK	5.55 ± 0.23	80.2 ± 26.5	14.5
6		L-Trp	L-Nle	L-Leu-EK	3.11 ± 0.026	3.27 ± 1.29	1.05
7		L-Phe	L-Nle	L-Phe-EK	6.70 ± 0.45	30.8 ± 13.7	4.60
8		Pyr-L-Ala	L-Nle	L-Phe-EK	3.87 ± 1.37	< 0.283	0.07
9		4-NH ₂ -L-Phe	L-Nle	L-Phe-EK	81.8 ± 14.0	3410 ± 2310	41.7
10		4-Boc-NH-L-Phe	L-Nle	L-Phe-EK	5.45 ± 2.49	478 ± 126	87.7
11		L-Trp	L-Nle	L-Phe-EK	9.77 ± 1.31	6.41 ± 2.26	0.66
12		4-Boc-NH-L-Phe	L-amino-Phe	L-Leu-EK	59.6 ± 15.4	0.91 ± 0.25	0.02
13		4-NH ₂ -L-Phe	L-amino-Phe	L-Phe-EK	68.2 ± 15.4	952 ± 275	14.0
14		4-Boc-NH-L-Phe	L-Boc-Phe	L-Leu-EK	13.5 ± 4.69	118 ± 21.7	8.74

15		4-Boc-NH-L-Phe	L-Boc-Phe	L-Phe-EK	12.2 ± 3.83	45.7 ± 15.7	3.75
16		L-Trp	L-Trp	L-Leu-EK	3.70 ± 0.14	11.7 ± 3.32	3.16
17		L-Trp	L-Trp	L-Phe-EK	9.38 ± 0.67	346 ± 86.2	36.9
18		D-Val	L-Nle	L-Leu-EK	3.27 ± 0.23	1240 ± 274	379.2
19		D-Trp	L-Nle	L-Leu-EK	2.92 ± 0.40	915 ± 289	313.4
20		D-Pyr-Ala	L-Nle	L-Leu-EK	21.8 ± 3.67	< 0.283	0.01

***In vitro* validation of carmaphycin B analogs**

Our cell based assays identified carmaphycin B analogs with selectivity indices ranging from 0.02 (analog **12**) to 379.2 (analog **18**). Therefore, we further evaluated the six compounds with selectivity indices of >30 in biochemical assays. To accomplish this, we first isolated the 20S *Plasmodium* proteasome (Pf20S) that was enriched from schizont lysate using a two-step column chromatography protocol (Figure S1). The concentration of Pf20S proteasome was determined based on subunit protein levels when compared to the human constitutive 20S (c20S) proteasome on a silver stained protein gel (Figure S1). Using 0.3 nM of each proteasome, we then compared proteolytic activity using well defined human proteasome substrates, z-LLE-AMC, z-LRR-AMC and suc-LLVY-AMC that are preferentially cleaved by the β 1, β 2 and β 5 subunits, respectively. When c20S was assayed in the presence of 150 nM carmaphycin B, β 5 activity was inhibited by

98% while $\beta 1$ and $\beta 2$ activity were reduced by 6% and 9%, respectively. These data clearly show that carmaphyacin B preferentially targets the human $\beta 5$ subunit. Pf20S hydrolyzed z-LRR-AMC and suc-LLVY-AMC at rates similar to the c20S (within 2-fold) while z-LLE-AMC activity by Pf20S was 19-fold lower than for c20S (Figure 2A). Addition of 150 nM carmaphyacin B resulted in $\beta 5$ activity being reduced by 45%, while $\beta 1$ and $\beta 2$ were reduced by 16% and 29%, respectively. Therefore, carmaphyacin B targets all three subunits of the *P. falciparum* proteasome but is a more potent inhibitor of the $\beta 5$ subunit.

Inhibition of the $\beta 5$ subunit was then evaluated using 50 nM of carmaphyacin B and the six *P. falciparum* selective analogs. For the human c20S, $\beta 5$ activity in the presence of carmaphyacin B and **1** was reduced by 97% and 89%, respectively, however analogs **18** and **19** were much less potent and decreased activity by 10% or less (Figure 2B). At 50 nM concentration, all compounds inhibited Pf20S $\beta 5$ activity by between 10 and 47% and only analog **18** was more potent towards Pf20S than c20S. Finally, analog **18** exhibited the same subunit specificity as carmaphyacin B, and addition of 450 nM of this compound resulted in a decrease in $\beta 5$ activity of 45%, while $\beta 1$ and $\beta 2$ were reduced by 6% and 9%, respectively (Figure 2C). Interestingly, analogs **18** and **1** differ by only the chirality of the P3 valine residue. Finally, these results were further confirmed in whole cell *in vitro* assays, where treatment of trophozoite-stage parasites with carmaphyacin B or the six analogs mentioned above all inhibited *P. falciparum* $\beta 5$ activity by 40-60% (Figure 3A).

Peptide epoxyketone proteasome inhibitors are irreversible and therefore their absolute potency is most accurately described by their inactivation kinetics (k_{inact}/K_i). The k_{inact}/K_i for carmaphyacin B was calculated to be $4,481 \text{ M}^{-1} \text{ s}^{-1}$ for c20S and 864.3 for Pf20S (Table 4). Substitution of L-methionine sulfone with L-norleucine in P2 in analog **1** results in a 3-fold loss in potency to c20S ($1500.3 \text{ M}^{-1} \text{ s}^{-1}$) and no significant change to Pf20S ($767.7 \text{ M}^{-1} \text{ s}^{-1}$). However, substitution of the P3 L-valine in **1** with D-valine in **18** resulted in a 100-fold loss in potency to the human c20S proteasome but only a 10-fold reduction to the Pf20S proteasome. The 10-fold larger decrease in inhibition of the human proteasome clearly indicates that, at least in part, the decrease in toxicity of analog **18** is due to decreased affinity for the human $\beta 5$ subunit of the proteasome, rather than other factors, such as decreased uptake of analog **18**. Furthermore, these data confirmed that our modifications of the P2 and P3 residues of carmaphyacin B resulted in the design of a peptide epoxyketone (analog **18**) that selectively inhibits the *Plasmodium* proteasome.

Table 4: Calculation of inactivation kinetics for carmaphycin B and analogs **1** and **18**

Compound	c20S			Pf20S		
	CarB	1	18	CarB	1	18
k_{inact} (s ⁻¹)	1.68×10 ⁻³	5.62×10 ⁻³	6.2×10 ⁻⁴	1.92×10 ⁻⁴	1.76×10 ⁻³	5.88×10 ⁻⁵
K_i (nM)	374.9	3,744	39,213	222.6	2,294	371.7
k_{inact}/K_i (M ⁻¹ s ⁻¹)	4,481	1500.3	15.8	864.3	767.7	158.1

Carmaphycin B synergy with Artemisinin

In *Plasmodium falciparum*, artemisinin (ART) treatment induces growth retardation and accumulation of ubiquitinated proteins, indicating that this family of drugs activates the cell stress response and saturates the ability of the proteasome to degrade these proteins. ART-resistant parasites cope with higher levels of ubiquitinated proteins by increasing substrate turnover using the parasite proteasome. Unsurprisingly, co-treatment of parasites with dihydroartemisinin and clinically approved proteasome inhibitors strongly synergize artemisinin activity against both Artemisinin sensitive and Artemisinin resistant strains ¹¹. Based upon this recognized synergy, we wanted to determine whether carmaphycin B and analog **18** also shared similar synergistic properties. When wild-type artemisinin-sensitive Dd2 parasites were treated with artemisinin we obtained an IC₅₀ of between 19.0 and 23.5 nM. Co-treatment of wild-type parasites with ART and 0.5 and 1 nM of carmaphycin B resulted in 2-fold and 3-fold sensitization to ART (Figure 3B). In addition, co-treatment with ART and 0.5 and 1 nM of analog **18** (Figure 3C) yielded a similar increase in ART sensitivity. These concentrations were selected to not significantly affect parasite growth, and we observed <10% inhibition of SYBR green signal with treatment with carmaphycin B or analog **18** at the two indicated concentrations.

Selectivity modeling of Carmaphycin B / Analog **18** towards the human $\beta 5$ binding pocket and the model of the Pf $\beta 5$ binding pocket

To better understand the molecular basis for the observed specificity of compound **18** towards the *Plasmodium* 20S proteasome $\beta 5$ subunit, we investigated the binding mode of carmaphycin B and **18** towards the human and the parasite proteasome using molecular modeling approaches. We created a homology model system of the *Plasmodium* 20S proteasome $\beta 5$ and $\beta 6$ subunits (homPf_ $\beta 5$ and homPf_ $\beta 6$) based on the crystal structure of the homologous human 20S proteasome (PDB ID 4R67) and the *Plasmodium* 20S proteasome cryo-EM structure (PDB ID 5FMG) ³²⁻³³. In addition, sequence alignment of the *Plasmodium* and human $\beta 5$ and $\beta 6$ protein chains provided valuable information about modifications that could be responsible

for differences in substrate specificity. Using molecular docking experiments in combination with the sequence alignment, we were able to identify key residues that contribute to the binding differences (Table S4, Figure S2).

The binding pose of carmaphycin A to the yeast 20S proteasome $\beta 5$ subunit was described earlier (Figure 1) and was used as starting point for our analysis²¹. In molecular docking experiments, we observed a very similar binding mode of carmaphycin B in the human and *Plasmodium* 20S proteasome $\beta 5$ subunit³⁴. In contrast, the molecular docking experiments of compound **18** revealed a switch in the binding position of **18** as a result of the altered stereochemistry of the P3 D-valine residue (Figure 4). In this switched position, the P4 fatty acid residue occupies the S3 binding pocket whereas the P3 residue is exposed to the inner cavity of the protein complex. The human S3 pocket is also more restricted in length whereas the parasite S3 pocket has a longer pore-like structure. This structure of the *Plasmodium* S3 pocket is therefore more likely to accommodate the long lipophilic hexanoate residue of compound **18** in the switched position than the human S3 pocket. This switched binding position was previously observed for P3 D-Ala containing compounds binding to the yeast 20S proteasome $\beta 5$ subunit³¹.

Conclusions

Proteasome inhibitors have shown excellent potential as antimalarial compounds, particularly in light of their synergy with artemisinin's mechanism of action. This study reports on our efforts to design and evaluate proteasome inhibitors based on the carmaphycin B scaffold, and to identify analogs that have potent antimalarial activity with low host cytotoxicity. Our lead compound, analog **18**, has a 100-fold wider therapeutic window than carmaphycin B and consists of the substitutions of D-valine for L-valine, and norleucine for methionine sulfone. We show that this compound retains potent antimalarial activity in cell-based assays against both asexual blood stages and gametocytes, and strongly inhibits the activity of the isolated *Plasmodium* proteasome *in vitro*. Moreover, *in vitro* evolution in *S. cerevisiae*, biochemical assays and molecular modeling studies confirm that this activity is due to specific inhibition of the $\beta 5$ subunit of the proteasome.

The rational inhibitor design used in this study was focused on developing compounds with reduced toxicity to human cells. We have clearly shown that introducing a D-amino acid in the P3 position can

significantly alter host cytotoxicity without greatly interfering with anti-*Plasmodial* activity. Our molecular modeling of this compound with the $\beta 5$ -subunit of the human and parasite proteasome determined that subtle structural differences in the Pf20S $\beta 5$ -subunit active site permit this selectivity and provide the structural basis for the design of more parasite-specific proteasome inhibitors. This insight will prove critical as more inhibitors are developed in the treatment of malaria and other tropical parasitic diseases.

An essential characteristic of any future anti-malarial compounds is that it has oral bioavailability. An oral proteasome inhibitor has been approved for treatment of multiple myeloma that consists of a prodrug that is released under aqueous conditions into a peptide boronic acid proteasome inhibitor. In addition, two orally bioavailable epoxyketone inhibitors have been developed that have potent antimyeloma activity³⁵⁻³⁶. One of these inhibitors, ONX 0912³⁵, is in Phase 1 clinical trial. These anti-cancer drug studies will provide the framework for design of anti-*Plasmodial* proteasome inhibitors with good pharmacokinetic and pharmacodynamic properties.

Experimental Methods

***S. cerevisiae* susceptibility and dose-response assay**

ABC₁₆-Monster yeast cells¹⁵ were inoculated into 5 ml of liquid YPD media and grown to saturation ($OD_{600} > 1.0$) overnight at 200 RPM in a shaking incubator at 30°C. Cultures were diluted to OD_{600} 0.005 to log phase. 100 μ l of yeast cells were added to a 96-well plate and incubated with compound starting with a concentration of 150 μ M, followed by 1:2 serial dilutions. An initial reading of OD_{600} ($t = 0$ hrs) was recorded using a Synergy HT spectrophotometer, and cells were grown for a period of 18 hours at 30°C. After incubation, plates were read at OD_{600} . Cells grown in the absence of compound were used as a negative control. Percent growth was calculated using the formula $OD_{600\text{treated}}/OD_{600\text{control}} \times 100$

IC_{50} values were determined by first subtracting the OD_{600} values at $t=0$ from those of the final reading and then using Prism 6 (GraphPad Software Inc) to calculate nonlinear regression on $\log(\text{inhibitor})$ vs. response with variable slope (four parameters).

Selection of Carmaphycin B-resistant *S. cerevisiae*

Varied concentrations of carmaphycin B were added to 50 ml conical tubes containing 20 μ l of saturated ABC₁₆-Monster cells in 20 ml of YPD media. Each selection was cultured under vigorous shaking until the culture reached saturation. Saturated cultures were diluted into fresh YPD media containing carmaphycin B, and multiple rounds of selection under increased drug pressure were performed. Cells of cultures that were able to grow in substantially higher drug concentrations than the parental cell line, were streaked onto agar plates containing carmaphycin B to select for colonies. Single colonies were isolated, and IC₅₀ assays, prepared by two-fold dilution from 150 μ M to 1.17 μ M were performed to determine the degree of evolved resistance vs. that of the parental strain.

Whole-genome sequencing and analysis

For whole-genome sequencing (WGS), DNA was extracted from yeast cells using the YeaStar Genomic DNA kit. Genomic yeast DNA libraries were normalized to 0.2 ng/ μ L and prepared for sequencing according to the manufacturer's instructions using the Illumina Nextera XT kit whole-genome resequencing library (Illumina, Inc., San Diego). DNA libraries were clustered and run on an Illumina HiSeq as 2x100 paired end reads, according to the manufacturer's instructions. Base calls were made using the software CASAVA v1.8.2. Initial sequence alignments were performed using the PLaTyPuS software³⁷. Reads were aligned to the reference *S. cerevisiae* genome using BWA, and unmapped reads were filtered using SAMTools. SNVs were called using GATK and filtered using the PLaTyPuS software³⁷.

Accession Codes

Sequences have been placed in the short-read sequence archive (<http://www.ncbi.nlm.nih.gov/sra>) under accession code SAMN06345855 for lineage 1, SAMN06345856 for lineage 2 and SAMN06345857 for lineage 3.

***P. falciparum* culture**

P. falciparum Dd2 strain parasites were cultured under standard conditions³⁸, using RPMI media supplemented with 0.05 mg/ml gentamycin, 0.014 mg/ml hypoxanthine (prepared fresh), 38.4 mM HEPES, 0.2% Sodium Bicarbonate, 3.4 mM Sodium Hydroxide, 0.05% O+ Human Serum (Denatured at 56°C for 40

min and From Interstate Blood Bank, Memphis, TN) and 0.0025% Albumax). Human O+ whole blood was obtained from TSRI blood bank (La Jolla, CA). Leukocyte-free erythrocytes are stored at 50% hematocrit in RPMI-1640 screening media (as above, but without O+ human serum and with 2x albumax concentration) at 4°C for one to three weeks before experimental use. Cultures were monitored every one to two days via direct observation of parasite infection using light microscopy-based observation of giemsa-stained thin blood smears of parasite cultures.

Compound sensitivity assay using SYBR® Green I

Compound susceptibility was measured using the malaria SYBR Green I-based fluorescence assay ³⁹. Asynchronous *P. falciparum* parasites (Dd2 strain) were cultured in standard conditions before being plated for the assays. Each compound was tested over 72 hours in technical duplicates on a twelve-point concentration curve prepared by three-fold dilution from 6.7 µM to 0.11 nM. At least three independent experiments were carried out for IC₅₀ determination. Artemisinin and chloroquine were used as controls. IC₅₀ values were obtained using normalized fluorescence intensity from SYBR green I and analyzed via non-linear variable slope four-parameter regression curve-fitting model in Prism 6 (GraphPad Software Inc).

***P. falciparum* induction and compound sensitivity testing of stage V gametocytes**

Gametocytes were induced in NF54 or derived clones as previously described ⁴⁰. Asexual blood stage parasites were synchronized at ring stage using 5% sorbitol for three consecutive life cycles. Once the culture reached a parasitemia of 8-10% ring stages, half of the media was exchanged to stress the parasites. Twenty-four hours later, the culture media was exchanged with fresh media and the culture was shaken overnight. The following day, the culture was treated with 50 mM N-acetyl-glucosamine (NAG) (in complete media), and new media containing NAG was added every day for 10 days to clear remaining asexual blood stage parasites and enrich for gametocytes. After 10 days, complete media without NAG was provided each day for the last two days of gametocyte development in order to obtain ~1% gametocytemia with >80% Stage V specificity and no visible asexual blood stage parasites (assessed via Giemsa-stained thin smears). Drug Sensitivity of Stage V gametocytes were then determined using a published protocol using mitotracker red ⁴¹. Each compound was tested in technical triplicate in a ten-point concentration curve prepared by three-fold dilution starting at 12.5

μM . At least three independent experiments were carried out for IC_{50} determination and puromycin was used as a positive control. IC_{50} values were obtained using the normalized bioluminescence intensity and a non-linear variable slope four-parameter regression curve-fitting model in Prism 6 (GraphPad Software Inc).

***P. berghei*-luciferase liver stage assay and HepG2 cytotoxicity assay**

The liver-stage and HepG2 toxicity assays were performed as previously reported⁴². Briefly, HepG2-A16-CD81EGFP were cultured at 37°C in 5% CO_2 in DMEM (Life Technologies, CA) supplemented with 10% FBS, 0.29 mg/ml glutamine, 100 unit penicillin and 100 $\mu\text{g}/\text{ml}$ streptomycin. For both the *P. berghei*-luciferase and HepG2 cytotoxicity assays, 3×10^3 of the HepG2-A16-CD81EGFP cells in 5 μl of culture medium (DMEM without Phenol Red (Life Technologies, CA), 5% FBS, and 5x Pen Strep Glutamine (Life Technologies, CA)) at concentration 6×10^5 cells/ml were seeded in 1536-well plates 24 hours prior to infection. 18 hours prior to infection, 50 nl of compound was transferred via Acoustic Transfer System (ATS) (Biosera) into the assay plates, and compounds were tested in technical duplicates on a twelve-point concentration curve prepared by three-fold dilution from 10.0 μM to 0.15 nM. Atovaquone and Puromycin were used as positive controls for *P. berghei* and HepG2 cytotoxicity respectively.

An. stephensi mosquitoes, infected with *P. berghei*-luciferase, were provided by the New York University Insectary. *P. berghei*-luciferase sporozoites were freshly dissected from the infected *A. stephensi* mosquito salivary glands, filtered, counted and then adjusted to final concentration 200 sporozoites per μl in the assay media. For the *P. berghei* assay, the HepG2-A16-CD81EGFP cells were infected with 1×10^3 sporozoites per well and the plates were spun down at 37°C for 3 minutes at 330g. The HepG2-A16-CD81EGFP cell designated for toxicity studies were left uninfected, with 5 μl of additional assay media added to each well to maintain equal concentrations of compounds. After 48 hours, exoerythrocytic growth and HepG2-A16-CD81EGFP cell viability were quantified by a bioluminescence measurement Envision Multilabel Reader (PerkinElmer). IC_{50} values were obtained using the normalized bioluminescence intensity and a non-linear variable slope four-parameter regression curve-fitting model in Prism 6 (GraphPad Software Inc).

Parasite isolation and protein extraction

Asynchronous *P. falciparum* cultures were grown up to 4-5% parasitemia, in 300 mL of RPMI media at 5.0% hematocrit. Cultures were then transferred to 50 ml conical tubes, pelleted via centrifugation at 800g for 5 min, and washed once with 1xPBS and pelleted again as above. The PBS was removed and lysis buffer (0.15% saponin in PBS) was added on ice in 10 pellet volumes. Upon lysis of red blood cells, indicated by a clear red supernatant, the lysed cultures were centrifuged at 3200 x g for 12 minutes at 4°C. The supernatant was removed by aspiration and the cells were washed twice using chilled PBS in microcentrifuge tubes. The cell pellets were then incubated on ice for 1 hour with occasional vortexing in a buffer consisting of 20 mM Tris-HCl pH 7.5, 5 mM MgCl₂, 1 mM DTT, 100 µM E-64 and 1 mM AEBSF. This sample was then subjected to 3 rounds of freezing (-80°C) and thawing (37°C) and centrifugation at 6000 x g for 10 min. The supernatant containing soluble *P. falciparum* protein was quantified by the BCA method (Pierce).

Enrichment of *P. falciparum* proteasome

P. falciparum proteasome was enriched by two-chromatographic steps reported previously¹⁰. In brief, 10 mg of *P. falciparum* protein was concentrated to 1 mL using a 100 kDa centrifugal filter unit (Amicon) and loaded onto a 5 ml anion exchange HiTrap DEAE FF column (GE healthcare). Protein was eluted using a linear gradient from 0 to 1 M NaCl and 1.5 ml fractions were collected and all fractions were assayed with 25 µM Succinyl-Leu-Leu-Val-Tyr-aminocoumarin (Suc-LLVY-AMC) in assay buffer (20 mM Tris pH 7.5, 0.02% SDS). The AMC fluorophore release was monitored at Ex 340/ Em 465 nm at 24°C using a Synergy HTX multi-mode reader (Biotek). Proteolytically active fractions were pooled and concentrated to 0.5 mL using a 100 kDa centrifugal filter unit (Amicon) and loaded onto a Superose 6 10/300 GL column (GE healthcare). Proteins were eluted using 20 mM Tris-HCl pH 7.5, 100 mM NaCl, 10% glycerol and 1 ml fractions were collected, evaluated for protease activity and pooled.

Proteasome activity assays

To estimate the concentration of Pf20S in the final pooled sample, protein was denatured and loaded into a 4-12% Bis-Tris Plus gel (Thermo Fisher Scientific) beside 60 to 100 ng of human constitutive proteasome (Boston Biochem). The gel was silver stained (Thermo Fisher Scientific) and Pf20S subunit concentration was estimated using Image J software. Proteasome activity assays were performed using 0.29

nM of Pf20S or c20S and 25 μ M of Suc-LLE-AMC, Suc-LRR-AMC or Suc-LLVY-AMC in assay buffer. For inhibition assays, inhibitor and substrate were added simultaneously to the enzyme and the rate of AMC release was determined from 60 to 120 minutes and compared to a DMSO control. To investigate which proteasome subunits are targeted by Carmaphycin B, assays were performed using 150 nM on inhibitor and the three substrates outlined above, and a similar evaluation was performed with analog **18** at 450 nM. Additional inhibition assays were performed using 50 nM of compounds and only Suc-LLVY-AMC.

Evaluation of on-target proteasome inhibition

Sorbitol synchronized early trophozoite parasites at 5% parasitemia were incubated with 95 nM of inhibitors for 4 hr. Parasites were washed and protein lysates were prepared as described above. 15 μ g of total protein was combined with 25 μ M Suc-LLVY-AMC in assay buffer and activity was evaluated as outlined above. Inhibition of proteasome activity was compared to DMSO treated cells.

Calculation of inhibition constants

To calculate inhibition constants, activity assays were performed as described above except using 200 μ M Suc-LLVY-AMC substrate. The rate of AMC release was calculated in the presence of serial dilution of each inhibitor. The rate of product formation was calculated at 30 min intervals for 4 hours, and normalized to activity DMSO control to calculate inactivation curves. K_{obs} values for each inhibitor concentration were calculated from inactivation curves, and inhibition constants K_i and k_{inact} were calculated by non-linear regression of K_{obs} and inhibitor concentration using GraphPad Prism 6 software.

Molecular Modeling

Molecular Operating Environment (MOE) 2016.08 (Chemical Computing Group, Montreal, QC, Canada) was used to perform the molecular modeling experiments and to create all pictures. The Amber10: EHT force field as implemented in MOE was used for all energy minimization calculations. All covalent docking experiments were performed using the Docktite application⁴³. The pharmacophore method with London dG scoring was used for placement of the ligands and refined with the induced fit method with GBVI/WSA dG

rescoring. The docking application was adapted to the binding of a seven-membered ring system instead of a 6-membered ring system to comply with the most recent literature ³⁴.

Mutant modeling: The yeast proteasomal crystal structure in complex with carmaphycin A (PDB ID 4HRD) was used as a template for mutation modeling analysis. PDB ID 4HRD chain K complies with proteasome component PRE2 (PRE2 sequence position 76-287 = PDB residue 1-212). The M45 residue was mutated with the Protein Builder and the resulting model was energy minimized. The $\beta 5$ and $\beta 6$ subunit together with crystal water molecules in a radius of 4.5Å from receptor or ligand were used for further analysis.

Homology model: The homology model system of the *Plasmodium* 20S proteasome $\beta 5$ and $\beta 6$ subunits (homPf_b5) was created based on the crystal structure of the homologous human 20S proteasome (PDB ID 4R67) and the sequence information of the *Plasmodium* 20S proteasome cryo-EM structure (PDB ID 5FMG). The human 20S proteasome was used as template and the individual subunits were aligned to construct several models of the Pf 20S proteasome. The models were scored using the GB/VI scoring method and the final model was protonated with Pronotate3D and energy minimized to an RMS gradient of 0.5. The geometry of the homology model was examined.

Analog Synthesis

In order to obtain the 20 analogs described in this study, we utilized a convergent, flexible and scalable synthesis procedure that avoids racemization, a common problem in the synthesis of peptide-like structures. The synthesis of these analogues was divided into two parts, the leucine-EK part (P1) and the dipeptide part which contains the P2-P3-P4 moieties, and each of these two parts was synthesized separately according to a previously established procedure. The synthesis was completed by attaching the Leu-EK moiety (P1) to the desired dipeptide moiety (P2-P3-P4) using simple HBTU/HOBt coupling to afford the desired analogues. In case of Boc-protected compounds **4**, **10**, **12** and **14**, the protecting group was cleaved by TFA/DCM and the crude compound was purified on RP-HPLC to afford their free amine analogues **5**, **9**, **13**, **15**.

A solution of intermediate (0.2 mmol, 1 equiv.) and LiOH.H₂O (2.0 mmol, 10 equiv.) in 1,4-dioxane/H₂O (20 mL, 2:1) was stirred at 25 °C. After 1.5 h, all volatiles were evaporated off and the resulting residue was suspended in H₂O (10 ml), acidified and extracted with EtOAc (3 x 10 ml). The combined organic extracts were dried using anhydrous sodium sulfate and concentrated to obtain the free acid of the intermediate as a white

solid. In a separate reaction, Boc-L- epoxyketone derivatives (0.7 mmol) in CH₂Cl₂ (5 ml) was treated with TFA (1 ml, 13.0 mmol) and stirred at 25°C for 1 h, whereupon it was concentrated in vacuo to a reddish oil. A fraction of this oil (0.14 mmol, 1.2 equiv) was dissolved in CH₂Cl₂ (2 ml) and added to a solution of the previously prepared free acid (0.12 mmol, 1.0 equiv) and HBTU (0.14 mmol, 1.2 equiv) in CH₂Cl₂ (10 ml) at 25°C; followed by addition of DiPEA (0.264 mmol, 2.2 equiv). After stirring for 3-5 h at 25°C, the reaction mixture was quenched with saturated NH₄Cl, followed by solvent partition and CH₂Cl₂ (3 x 15 ml) extractions of the aqueous layer. All organic extracts were combined and dried using anhydrous sodium sulfate, and concentrated in vacuo. Silica gel column chromatography (10-100% EtOAc/hexanes) yielded pure compounds **1-20**.

A Jasco P-2000 polarimeter was used to measure optical rotations. NMR spectra were recorded on a Bruker 500 MHz spectrometer (500 and 125 MHz for the ¹H and ¹³C nuclei, respectively) using CDCl₃ or CD₃OD as solvent from Cambridge Isotope Laboratories, Inc. (99.8% D). Spectra were referenced to residual CDCl₃ solvent as internal standard (δ_H 7.26 and δ_C 77.1). LC-HRMS data for analysis of compounds **1-20** were obtained on an Agilent 6239 HR-ESI-TOFMS equipped with a Phenomenex Luna 5 μM C18 100 Å column (4.6 x 250 mm). Semi-preparative HPLC purification was carried out using a Waters 515 with a Waters 996 photodiode array detector using Empower Pro software. All solvents were HPLC grade.

Analytical data and SMILES strings are available for all analogs in the supplementary material and ¹H and ¹³C NMR traces for analogs **18** and **19** are displayed in Figures S3-S6. Purity was assessed by HPLC and all compounds possessed greater than 95% purity.

Acknowledgements

We would like to thank the members of the Winzeler, O'Donoghue and Gerwick labs for advice and critical reading of the manuscript. G.L. is supported by an A.P. Giannini Post-Doctoral Fellowship. S.O. and G.M.G. are supported by the Bill and Melinda Gates Foundation, Grand Challenge in Global Health Exploration Grant (OPP1086217, OPP1141300). G.M.G. is also supported by the UC San Diego Medical Scientist Training Program (T32 GM007198-40) and the DoD National Defense Science and Engineering Fellowship Program.

L.K. is supported by a research fellowship of the Deutsche Forschungsgemeinschaft (KE 2172/3-1). A.J.O is supported by lab start-up funds from the Skaggs School of Pharmacy and Pharmaceutical Sciences, UC San Diego. E.A.W. is supported by grants from the NIH (5R01AI090141 and R01AI103058). W.H.G. is supported by NIH grants GM107550 and AI127505.

Author Contributions

G.L., J.A., B.B.-V., L.K.; A.J.O., E.A.W., L.G., W.H. G., and S.O. designed the experiments and wrote the manuscript. Directed-evolution experiments and yeast IC₅₀ experiments were designed and performed by S.O., G.M.G., E.V., and J.Y. Whole-genome sequencing was performed by the UCSD Institute for Genomic Medicine Core Facility. Sequence analysis was performed by S.O. and J.Y. IC₅₀ experiments in parasites were designed and performed by G.L., B.Z, L.W, Y.A, P.O.S., C.A.B., S.O. and E.A.W. Chemical synthesis of compounds was designed and performed by J.A. and W.H.G. Computational docking studies were designed and performed by L.K. and W.H.G. Biochemical assays were performed, designed, and conducted by B.B.-V. and A.J.O. All authors read and approved the manuscript. The authors declare no conflict of interest. The authors will also release the atomic coordinates and experimental data for the homology models upon publication.

Corresponding Author Information

Sabine Otilie: Email: saottilie@ucsd.edu; Phone: 1-858-822-3601

Elizabeth Winzeler: Email: ewinzeler@ucsd.edu; Phone: 1-858-822-3339

William Gerwick: Email: wgerwick@ucsd.edu; Phone: 1-858-534-0578

Anthony O'Donoghue: Email: ajodonoghue@ucsd.edu; Phone: 1-858-534-5360

Abbreviations

CarB: carmaphycin B; *P. falciparum*: *Plasmodium falciparum*; *P. berghei*: *Plasmodium berghei*; GM: ABC₁₆⁻ Monster yeast strain; vs: vinyl-sulfone; Pf20S: *Plasmodium falciparum* 20S proteasome; c20S: constitutive human 20S proteasome; ART: artemisinin; CQ: chloroquine; homPf_β5: homology model system of the *Plasmodium* 20S proteasome β5 subunit; homPf_β6: homology model system of the *Plasmodium* 20S

proteasome $\beta 6$ subunit; s.e.m.: standard error of the mean; YPD: yeast extract peptone dextrose; WGS: whole genome sequencing.

References

1. World Health Organization. World Malaria Report: 2016. **2017**.
2. Dondorp, A. M.; Nosten, F.; Yi, P.; Das, D.; Phyto, A. P.; Tarning, J.; Lwin, K. M.; Ariey, F.; Hanpithakpong, W.; Lee, S. J.; Ringwald, P.; Silamut, K.; Imwong, M.; Chotivanich, K.; Lim, P.; Herdman, T.; An, S. S.; Yeung, S.; Singhasivanon, P.; Day, N. P.; Lindegardh, N.; Socheat, D.; White, N. J. Artemisinin resistance in *Plasmodium falciparum* malaria. *N Engl J Med* **2009**, *361* (5), 455-467.
3. Ariey, F.; Witkowski, B.; Amaratunga, C.; Beghain, J.; Langlois, A. C.; Khim, N.; Kim, S.; Duru, V.; Bouchier, C.; Ma, L.; Lim, P.; Leang, R.; Duong, S.; Sreng, S.; Suon, S.; Chuor, C. M.; Bout, D. M.; Menard, S.; Rogers, W. O.; Genton, B.; Fandeur, T.; Miotto, O.; Ringwald, P.; Le Bras, J.; Berry, A.; Barale, J. C.; Fairhurst, R. M.; Benoit-Vical, F.; Mercereau-Puijalon, O.; Menard, D. A molecular marker of artemisinin-resistant *Plasmodium falciparum* malaria. *Nature* **2014**, *505* (7481), 50-55.
4. Hovlid, M. L.; Winzeler, E. A. Phenotypic screens in antimalarial drug discovery. *Trends in parasitology* **2016**, *32* (9), 697-707.
5. Love, M. S.; Beasley, F. C.; Jumani, R. S.; Wright, T. M.; Chatterjee, A. K.; Huston, C. D.; Schultz, P. G.; McNamara, C. W. A high-throughput phenotypic screen identifies clofazimine as a potential treatment for cryptosporidiosis. *PLoS Negl Trop Dis* **2017**, *11* (2), e0005373.
6. Kato, N.; Comer, E.; Sakata-Kato, T.; Sharma, A.; Sharma, M.; Maetani, M.; Bastien, J.; Brancucci, N. M.; Bittker, J. A.; Corey, V.; Clarke, D.; Derbyshire, E. R.; Dornan, G. L.; Duffy, S.; Eckley, S.; Itoe, M. A.; Koolen, K. M.; Lewis, T. A.; Lui, P. S.; Lukens, A. K.; Lund, E.; March, S.; Meibalan, E.; Meier, B. C.; McPhail, J. A.; Mitasev, B.; Moss, E. L.; Sayes, M.; Van Gessel, Y.; Wawer, M. J.; Yoshinaga, T.; Zeeman, A. M.; Avery, V. M.; Bhatia, S. N.; Burke, J. E.; Catteruccia, F.; Clardy, J. C.; Clemons, P. A.; Dechering, K. J.; Duvall, J. R.; Foley, M. A.; Gusovsky, F.; Kocken, C. H.; Marti, M.; Morningstar, M. L.; Munoz, B.; Neafsey, D. E.; Sharma, A.; Winzeler, E. A.; Wirth, D. F.; Scherer, C. A.; Schreiber, S. L. Diversity-oriented synthesis yields novel multistage antimalarial inhibitors. *Nature* **2016**, *538* (7625), 344-349.
7. Newman, D. J.; Cragg, G. M. Natural Products as sources of new drugs from 1981 to 2014. *Journal of natural products* **2016**, *79* (3), 629-661.
8. Wells, T. N. Natural products as starting points for future anti-malarial therapies: going back to our roots? *Malaria journal* **2011**, *10 Suppl 1*, S3.
9. Pereira, A. R.; Kale, A. J.; Fenley, A. T.; Byrum, T.; Debonisi, H. M.; Gilson, M. K.; Valeriote, F. A.; Moore, B. S.; Gerwick, W. H. The carmaphycins: new proteasome inhibitors exhibiting an alpha,beta-epoxyketone warhead from a marine cyanobacterium. *Chembiochem* **2012**, *13* (6), 810-817.
10. Li, H.; Ponder, E. L.; Verdoes, M.; Asbjornsdottir, K. H.; Deu, E.; Edgington, L. E.; Lee, J. T.; Kirk, C. J.; Demo, S. D.; Williamson, K. C.; Bogyo, M. Validation of the proteasome as a therapeutic target in *Plasmodium* using an epoxyketone inhibitor with parasite-specific toxicity. *Chemistry & biology* **2012**, *19*, 1535-1545.
11. Dogovski, C.; Xie, S. C.; Burgio, G.; Bridgford, J.; Mok, S.; McCaw, J. M.; Chotivanich, K.; Kenny, S.; Gnadig, N.; Straimer, J.; Bozdech, Z.; Fidock, D. A.; Simpson, J. A.; Dondorp, A. M.; Foote, S.; Klonis, N.; Tilley, L. Targeting the cell stress response of *Plasmodium falciparum* to overcome artemisinin resistance. *PLoS Biol* **2015**, *13* (4), e1002132.
12. Infante, J. R.; Mendelson, D. S.; Burris, H. A., 3rd; Bendell, J. C.; Tolcher, A. W.; Gordon, M. S.; Gillenwater, H. H.; Arastu-Kapur, S.; Wong, H. L.; Papadopoulos, K. P. A first-in-human dose-escalation study of the oral proteasome inhibitor oprozomib in patients with advanced solid tumors. *Investigational new drugs* **2016**, *34* (2), 216-224.

13. Bibo-Verdugo, B.; Jiang, Z.; Caffrey, C. R.; O'Donoghue, A. J. Targeting proteasomes in infectious organisms to combat disease. *The FEBS journal* **2017** *284*,1503-1517.
14. Otilie, S.; Goldgof, G. M.; Calvet, C. M.; Jennings, G. K.; LaMonte, G.; Schenken, J.; Vigil, E.; Kumar, P.; McCall, L. I.; Lopes, E. S.; Gunawan, F.; Yang, J.; Suzuki, Y.; Siqueira-Neto, J. L.; McKerrow, J. H.; Amaro, R. E.; Podust, L. M.; Durrant, J. D.; Winzeler, E. A. Rapid chagas disease drug target discovery using directed evolution in drug-sensitive yeast. *ACS chemical biology* **2017**, *12* (2), 422-434.
15. Goldgof, G. M.; Durrant, J. D.; Otilie, S.; Vigil, E.; Allen, K. E.; Gunawan, F.; Kostylev, M.; Henderson, K. A.; Yang, J.; Schenken, J.; LaMonte, G. M.; Manary, M. J.; Murao, A.; Nachon, M.; Stanhope, R.; Prescott, M.; McNamara, C. W.; Slayman, C. W.; Amaro, R. E.; Suzuki, Y.; Winzeler, E. A. Comparative chemical genomics reveal that the spiroindolone antimalarial KAE609 (Cipargamin) is a P-type ATPase inhibitor. *Sci Rep* **2016**, *6*, 27806.
16. Suzuki, Y.; St Onge, R. P.; Mani, R.; King, O. D.; Heilbut, A.; Labunskyy, V. M.; Chen, W.; Pham, L.; Zhang, L. V.; Tong, A. H.; Nislow, C.; Giaever, G.; Gladyshev, V. N.; Vidal, M.; Schow, P.; Lehar, J.; Roth, F. P. Knocking out multigene redundancies via cycles of sexual assortment and fluorescence selection. *Nature methods* **2011**, *8* (2), 159-164.
17. Franke, N. E.; Niewerth, D.; Assaraf, Y. G.; van Meerloo, J.; Vojtekova, K.; van Zantwijk, C. H.; Zweegman, S.; Chan, E. T.; Kirk, C. J.; Geerke, D. P.; Schimmer, A. D.; Kaspers, G. J.; Jansen, G.; Cloos, J. Impaired bortezomib binding to mutant beta5 subunit of the proteasome is the underlying basis for bortezomib resistance in leukemia cells. *Leukemia* **2012**, *26* (4), 757-768.
18. Finley, D.; Ulrich, H. D.; Sommer, T.; Kaiser, P. The ubiquitin-proteasome system of *Saccharomyces cerevisiae*. *Genetics* **2012**, *192* (2), 319-360.
19. Amerik, A. Y.; Li, S. J.; Hochstrasser, M. Analysis of the deubiquitinating enzymes of the yeast *Saccharomyces cerevisiae*. *Biological chemistry* **2000**, *381* (9-10), 981-992.
20. Fang, N. N.; Zhu, M.; Rose, A.; Wu, K. P.; Mayor, T. Deubiquitinase activity is required for the proteasomal degradation of misfolded cytosolic proteins upon heat-stress. *Nat Commun* **2016**, *7*, 12907.
21. Waite, K. A.; De-La Mota-Peynado, A.; Vontz, G.; Roelofs, J. Starvation Induces Proteasome Autophagy with Different Pathways for Core and Regulatory Particles. *The Journal of biological chemistry* **2016**, *291* (7), 3239-3253.
22. Trivella, D. B.; Pereira, A. R.; Stein, M. L.; Kasai, Y.; Byrum, T.; Valeriote, F. A.; Tantillo, D. J.; Groll, M.; Gerwick, W. H.; Moore, B. S. Enzyme inhibition by hydroamination: design and mechanism of a hybrid carmaphycin-syringolin enone proteasome inhibitor. *Chemistry & biology* **2014**, *21* (6), 782-791.
23. Huber, E. M.; Heinemeyer, W.; Groll, M. Bortezomib-resistant mutant proteasomes: structural and biochemical evaluation with carfilzomib and ONX 0914. *Structure (London, England : 1993)* **2015**, *23* (2), 407-417.
24. Aboulaila, M.; Munkhjargal, T.; Sivakumar, T.; Ueno, A.; Nakano, Y.; Yokoyama, M.; Yoshinari, T.; Nagano, D.; Katayama, K.; El-Bahy, N.; Yokoyama, N.; Igarashi, I. Apicoplast-targeting antibacterials inhibit the growth of *Babesia* parasites. *Antimicrobial agents and chemotherapy* **2012**, *56* (6), 3196-3206.
25. Kreidenweiss, A.; Kreamsner, P. G.; Mordmuller, B. Comprehensive study of proteasome inhibitors against *Plasmodium falciparum* laboratory strains and field isolates from Gabon. *Malaria journal* **2008**, *7*, 187.
26. Czesny, B.; Goshu, S.; Cook, J. L.; Williamson, K. C., The proteasome inhibitor epoxomicin has potent *Plasmodium falciparum* gametocytocidal activity. *Antimicrobial agents and chemotherapy* **2009**, *53* (10), 4080-4085.
27. Li, H.; O'Donoghue, A. J.; van der Linden, W. A.; Xie, S. C.; Yoo, E.; Foe, I. T.; Tilley, L.; Craik, C. S.; da Fonseca, P. C.; Bogyo, M. Structure- and function-based design of *Plasmodium*-selective proteasome inhibitors. *Nature* **2016**, *530* (7589), 233-236.
28. Bromme, D.; Klaus, J. L.; Okamoto, K.; Rasnick, D.; Palmer, J. T. Peptidyl vinyl sulphones: a new class of potent and selective cysteine protease inhibitors: S2P2 specificity of human cathepsin O2 in comparison with cathepsins S and L. *The Biochemical journal* **1996**, *315* (Pt 1), 85-89.
29. Arastu-Kapur, S.; Anderl, J. L.; Kraus, M.; Parlati, F.; Shenk, K. D.; Lee, S. J.; Muchamuel, T.; Bennett, M. K.; Driessen, C.; Ball, A. J.; Kirk, C. J. Nonproteasomal targets of the proteasome inhibitors bortezomib and

- carfilzomib: a link to clinical adverse events. *Clinical cancer research : an official journal of the American Association for Cancer Research* **2011**, *17* (9), 2734-2743.
30. Kisselev, A. F.; van der Linden, W. A.; Overkleeft, H. S. Proteasome inhibitors: an expanding army attacking a unique target. *Chemistry & biology* **2012**, *19* (1), 99-115.
31. de Bruin, G.; Huber, E. M.; Xin, B. T.; van Rooden, E. J.; Al-Ayed, K.; Kim, K. B.; Kisselev, A. F.; Driessen, C.; van der Stelt, M.; van der Marel, G. A.; Groll, M.; Overkleeft, H. S. Structure-based design of beta1i or beta5i specific inhibitors of human immunoproteasomes. *J Med Chem* **2014**, *57* (14), 6197-6209.
32. Harshbarger, W.; Miller, C.; Diedrich, C.; Sacchettini, J. Crystal structure of the human 20S proteasome in complex with carfilzomib. *Structure* **2015**, *23* (2), 418-424.
33. Li, H.; Bogyo, M.; da Fonseca, P. C., The cryo-EM structure of the Plasmodium falciparum 20S proteasome and its use in the fight against malaria. *The FEBS journal* **2016**, *283* (23), 4238-4243.
34. Schrader, J.; Henneberg, F.; Mata, R. A.; Tittmann, K.; Schneider, T. R.; Stark, H.; Bourenkov, G.; Chari, A. The inhibition mechanism of human 20S proteasomes enables next-generation inhibitor design. *Science* **2016**, *353* (6299), 594-598.
35. Chauhan, D.; Singh, A. V.; Aujay, M.; Kirk, C. J.; Bandi, M.; Ciccarelli, B.; Raje, N.; Richardson, P.; Anderson, K. C. A novel orally active proteasome inhibitor ONX 0912 triggers in vitro and in vivo cytotoxicity in multiple myeloma. *Blood* **2010**, *116* (23), 4906-4915.
36. Wang, Z.; Dove, P.; Wang, X.; Shamas-Din, A.; Li, Z.; Nachman, A.; Oh, Y. J.; Hurren, R.; Ruschak, A.; Climie, S.; Press, B.; Griffin, C.; Undzys, E.; Aman, A.; Al-awar, R.; Kay, L. E.; O'Neill, D.; Trudel, S.; Slassi, M.; Schimmer, A. D. FV-162 is a novel, orally bioavailable, irreversible proteasome inhibitor with improved pharmacokinetics displaying preclinical efficacy with continuous daily dosing. *Cell death & disease* **2015**, *6*, e1815.
37. Manary, M. J.; Singhakul, S. S.; Flannery, E. L.; Bopp, S. E. R.; Corey, V. C.; Bright, A. T.; McNamara, C. W.; Walker, J. R.; Winzeler, E. A. Identification of pathogen genomic variants through an integrated pipeline. *Bmc Bioinformatics* **2014**, *15*, 63.
38. Trager, W.; Jensen, J. B. Human malaria parasites in continuous culture. *Science* **1979**, *193*, 673-675.
39. Smilkstein M.; Sriwilajaroen N.; Kelly JX.; Wilairat P.; Riscoe M. Simple and inexpensive fluorescence-based technique for high-throughput antimalarial drug screening. *Antimicrob Agents Chemother.* **2004**, *48*, 1803-18066.
40. Fivelman, Q. L.; McRobert, L.; Sharp, S.; Taylor, C. J.; Saeed, M.; Swales, C. A.; Sutherland, C. J.; Baker, D. A. Improved synchronous production of Plasmodium falciparum gametocytes in vitro. *Molecular and Biochemical Parasitology* **2007**, *154*, 119-123.
41. Plouffe, David M.; Wree, M.; Du, Alan Y.; Meister, S.; Li, F.; Patra, K.; Lubar, A.; Okitsu, Shinji L.; Flannery, Erika L.; Kato, N.; Tanaseichuk, O.; Comer, E.; Zhou, B.; Kuhen, K.; Zhou, Y.; Leroy, D.; Schreiber, Stuart L.; Scherer, Christina A.; Vinetz, J.; Winzeler, Elizabeth A. High-Throughput assay and discovery of small molecules that interrupt malaria transmission. *Cell host & microbe.* *19*, 114-126.
42. Swann, J.; Corey, V.; Scherer, C. A.; Kato, N.; Comer, E.; Maetani, M.; Antonova-Koch, Y.; Reimer, C.; Gagaring, K.; Ibanez, M.; Plouffe, D.; Zeeman, A. M.; Kocken, C. H.; McNamara, C. W.; Schreiber, S. L.; Campo, B.; Winzeler, E. A.; Meister, S. High-throughput luciferase-based assay for the discovery of therapeutics that prevent malaria. *ACS Infect Dis* **2016**, *2*, 281-293.
43. Scholz, C.; Knorr, S.; Hamacher, K.; Schmidt, B. DOCKTITE-a highly versatile step-by-step workflow for covalent docking and virtual screening in the molecular operating environment. *Journal of chemical information and modeling* **2015**, *55*, 398-406.

Figure Legends

Figure 1: Binding Mode of Carmaphycin B in the *Saccharomyces cerevisiae* 20S proteasome β 5 subunit. (A) Binding mode of carmaphycin B in the yeast wild type structure based on molecular docking of carmaphycin B into the yeast 20S proteasome:carmaphycin A co-crystal structure (PDB ID 4HRD) (B) Modeling of the mutation of residue Met45 to Ile45 leads to a steric clash between the P1 leucine and the mutated Ile45 residue. The mutated Ile45 residue penetrates the interaction surface of carmaphycin B preventing the efficient binding of the ligand. The interaction surface is color coded according to the lipophilicity of the molecule with hydrophobic (blue) and lipophilic (red) areas.

Figure 2: Inhibition of the Human (black bars) and *Plasmodium* proteasome (gray bars) by Carmaphycin B and 6 *Plasmodium* specific analogs: A) activity against the 3 enzymatic subunits of Pf20S and the c20S. B) potency against c20S for carmaphycin B and the indicated compounds. C) Analog **18** compound activity against the 3 enzymatic subunits of Pf20S and the c20S. Results presented as mean \pm s.e.m with n=3.

Figure 3: On-target efficacy of proteasome inhibitors and synergistic activity with artemisinin. A) On-target studies with the synchronized trophozoite parasites for the indicated analogs. B) Artemisinin IC_{50} , as determined by 72 hour SYBR green assay, of Dd2 parasites when co-treated with the indicated concentrations of carmaphycin B. C) Artemisinin IC_{50} , as determined by 72 hour SYBR green assay, of Dd2 parasites when co-treated with the indicated concentrations of analog **18**. IC_{50} results presented as mean \pm s.e.m with n=2, with one representative regression curve shown.

Figure 4: Schematic representation of carmaphycin B (blue) and analog **18** (orange) in ball and stick representation bound to the human 20S proteasome β 5 binding pocket (left, PDB ID 4R67) and the *P. falciparum* 20S proteasome β 5 binding pocket of the homology model homPf_ β 5 (right). The molecular surface of the protein binding pocket is shown with hydrophilic (blue) and hydrophobic (red) surface areas. A) Carmaphycin B bound to the β 5 subunit. B) Analog **18** bound in the switched conformation. C) Analog **18** binding conformation in the S3 protein pocket. The residues that were identified to be associated with the preferred binding of analog **18** towards the *Plasmodium* 20S proteasome β 5 subunit are shown in grey. The

interaction surface of the inhibitor analog **18** is color coded according to the lipophilicity of the molecule with hydrophilic (blue) and hydrophobic (red) areas. D) Analog **18** binding conformation in the S3 protein pocket. The molecular surface of the S3 binding pocket is shown as a solid surface area whereas the whole binding pocket is shown as a line representation.

Figures

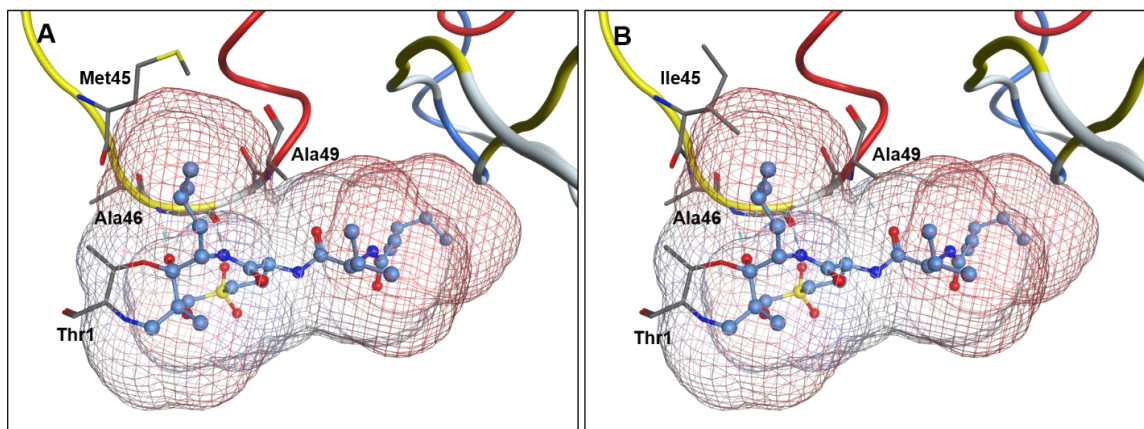


Figure 1: Binding Mode of Carmaphycin B in the *Saccharomyces cerevisiae* 20S proteasome $\beta 5$ subunit. (A) Binding mode of carmaphycin B in the yeast wild type structure based on molecular docking of carmaphycin B into the yeast 20S proteasome:carmaphycin A co-crystal structure (PDB ID 4HRD) (B) Modeling of the mutation of residue Met45 to Ile45 leads to a steric clash between the P1 leucine and the mutated Ile45 residue. The mutated Ile45 residue penetrates the interaction surface of carmaphycin B preventing the efficient binding of the ligand. The interaction surface is color coded according to the lipophilicity of the molecule with hydrophobic (blue) and lipophilic (red) areas.

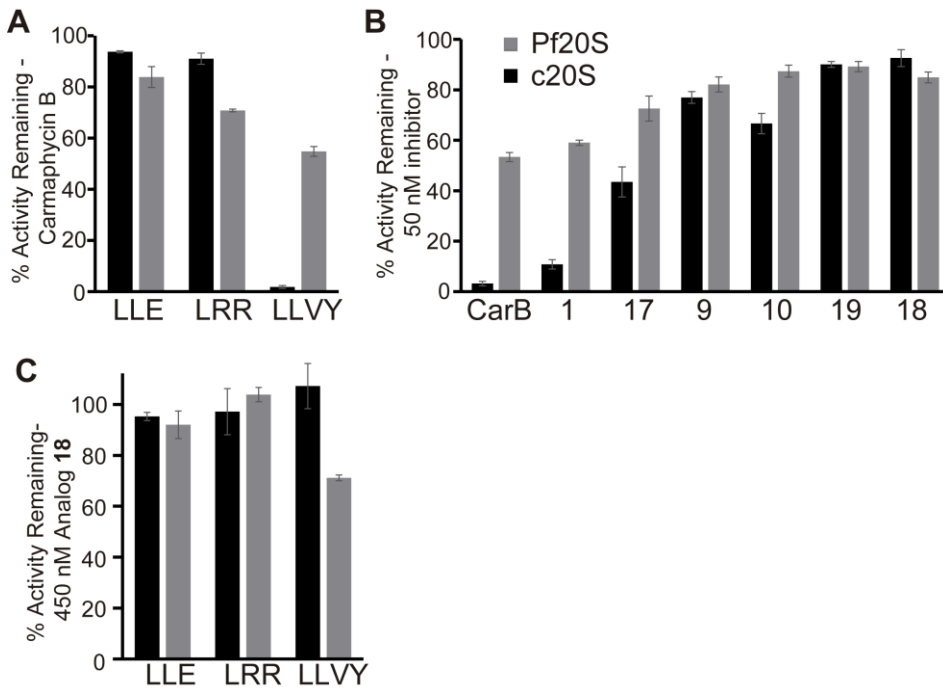


Figure 2: Inhibition of the Human (black bars) and *Plasmodium* proteasome (gray bars) by Carmaphycin B and 6 *Plasmodium* specific analogs: A) activity against the 3 enzymatic subunits of Pf20S and the c20S. B) potency against c20S for Carmaphycin B and the indicated compounds. C) Analog **18** compound activity against the 3 enzymatic subunits of Pf20S and the c20S. Results presented as mean \pm s.e.m with n=3.

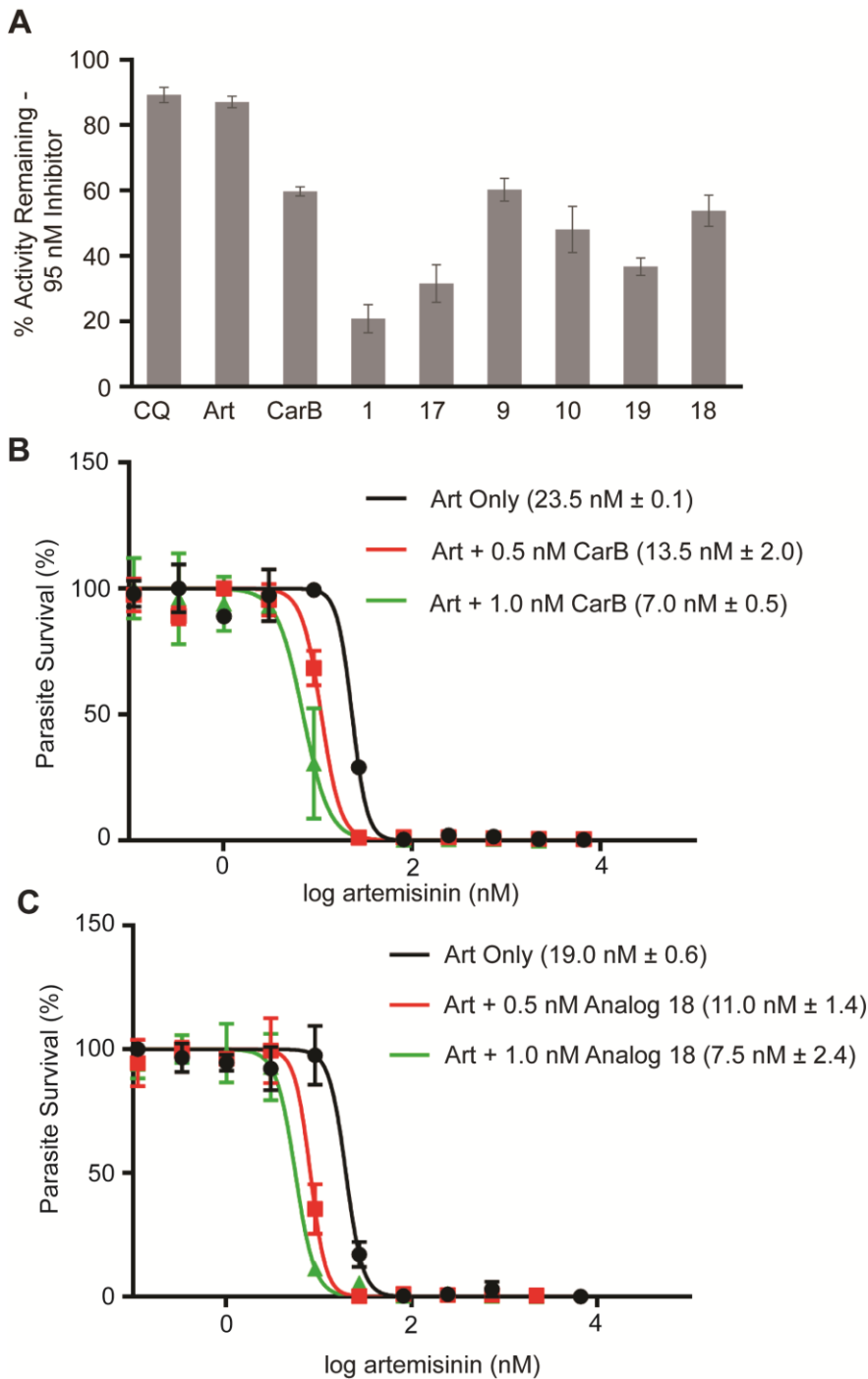


Figure 3: On-target efficacy of proteasome inhibitors and synergistic activity with artemisinin. A) On-target studies with the synchronized trophozoite parasites for the indicated analogs. B) Artemisinin IC_{50} , as determined by 72 hour SYBR green assay, of Dd2 parasites when co-treated with the indicated concentrations of carmaphycin B. C) Artemisinin IC_{50} , as determined by 72 hour SYBR green assay, of Dd2 parasites when co-treated with the indicated concentrations of analog **18**. IC_{50} results presented as mean \pm s.e.m with $n=2$, with one representative regression curve shown.

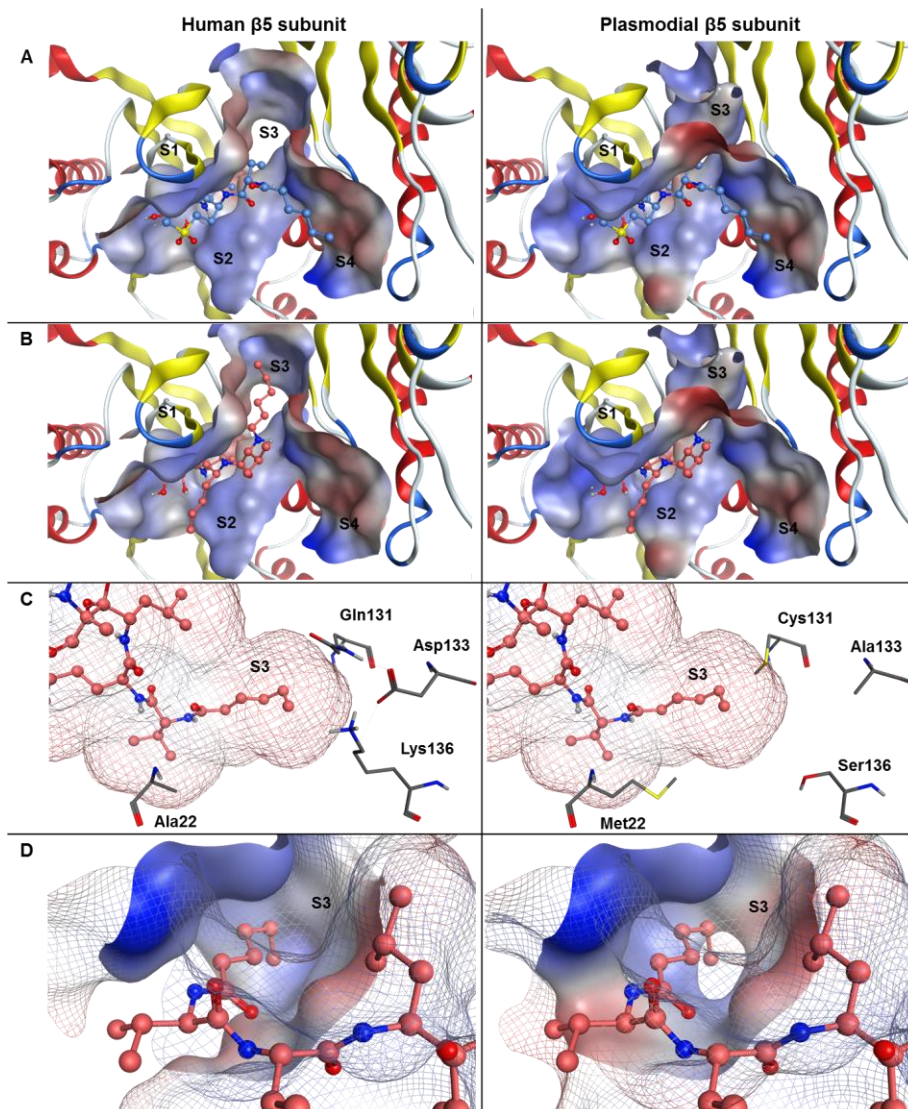
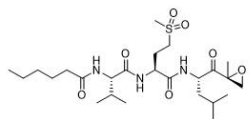
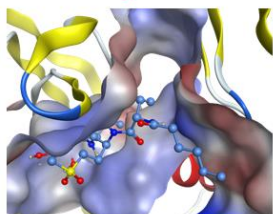


Figure 4: Schematic representation of carmaphycin B (blue) and analog **18** (orange) in ball and stick representation bound to the human 20S proteasome $\beta 5$ binding pocket (left, PDB ID 4R67) and the *P. falciparum* 20S proteasome $\beta 5$ binding pocket of the homology model homPf_ $\beta 5$ (right). The molecular surface of the protein binding pocket is shown with hydrophilic (blue) and hydrophobic (red) surface areas. A) Carmaphycin B bound to the $\beta 5$ subunit. B) Analog **18** bound in the switched conformation. C) Analog **18** binding conformation in the S3 protein pocket. The residues that were identified to be associated with the preferred binding of analog **18** towards the *Plasmodium* 20S proteasome $\beta 5$ subunit are shown in grey. The interaction surface of the inhibitor analog **18** is color coded according to the lipophilicity of the molecule with hydrophilic (blue) and hydrophobic (red) areas. D) Analog **18** binding conformation in the S3 protein pocket. The molecular surface of the S3 binding pocket is shown as solid surface areas whereas the whole binding pocket is shown as line representation.

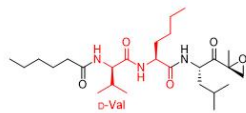
Table of Contents Graphic



Carmaphycin B
Selectivity Index = 3



SAR



Analog 18
Selectivity Index = 379

